

# ChatCAD+: Towards a Universal and Reliable Interactive CAD using LLMs

Zihao Zhao\*, Sheng Wang\*, Jinchen Gu\*, Yitao Zhu\*,  
Lanzhu Mei, Zixu Zhuang, Zhiming Cui, Qian Wang, Dinggang Shen, *Fellow, IEEE*

**Abstract**—The integration of Computer-Assisted Diagnosis (CAD) with Large Language Models (LLMs) holds great potential in clinical applications, specifically in the roles of virtual family doctors and clinic assistants. However, current works in this field are plagued by limitations, specifically a restricted scope of applicable image domains and the provision of unreliable medical advice. This restricts their overall processing capabilities. Furthermore, the mismatch in writing style between LLMs and radiologists undermines their practical usefulness. To tackle these challenges, we introduce ChatCAD+, which is designed to be universal and reliable. It is capable of handling medical images from diverse domains and leveraging up-to-date information from reputable medical websites to provide reliable medical advice. Additionally, it incorporates a template retrieval system that improves report generation performance via exemplar reports. This approach ensures greater consistency with the expertise of human professionals. The source code is available at [GitHub](#).

**Index Terms**—Large Language Models, Multi-modality System, Medical Dialogue, Computer-Assisted Diagnosis

## I. INTRODUCTION

LARGE Language Models (LLMs) have emerged as promising tools in various domains. It refers to advanced artificial intelligence that has been extensively trained on text data. Drawing on the combined power of sophisticated deep learning techniques, large-scale datasets, and increased model sizes, LLMs demonstrate extraordinary capabilities in understanding and generating human-like text. This is substantiated by significant projects like ChatGPT [1], LLaMA [2], and Open-Assistant [3]. These techniques are highly suitable for a wide range of scenarios, such as customer service, marketing,

education, and healthcare consultation. Notably, ChatGPT has passed part of the US medical licensing exams, highlighting the potential of LLMs in the medical domain [4]–[8].

So far, several studies have been conducted to integrate LLMs into Computer-Assisted Diagnosis (CAD) systems of medical images. Conventional CAD typically operates following pure computer vision [9]–[11] or vision-language paradigms [12], [13]. LLMs have shown the ability to effectively interpret findings from medical images, thus mitigating the limitations of only visual interpretation. For example, in our pilot study, we leverage the intermediate results obtained from image CAD networks and then utilize LLMs to generate the final diagnostic reports [14].

Although some efforts have been made to combine CAD networks and LLMs [14]–[16], it should be noted that these studies are limited in their scopes, which often focus on specific image domains. That is, such a system may only support a single image modality, a single organ, or a single application (such as Chest X-ray), which greatly limits the generalizability in the real clinical workflow. The primary reason for this limitation comes from the notable topologic and semantic variations observed among medical image modalities and organs, which present distinct challenges when attempting to encode various images with a single model.

Furthermore, LLMs often generate diagnostic reports that exhibit discrepancy in writing style when compared to those produced by real human experts [14], implying the lack of expertise of general LLMs in the field of diagnostics. It is also articulable that the integration of LLMs and CADs may lead to medical dialogue systems [17]–[20]. In this way, patients will be able to interact through LLMs and acquire more medical advice and explanation, while this functionality is often missing in conventional CAD systems. However, existing studies show that the general LLMs typically produce medical advice based solely on their encoded knowledge, without considering specific knowledge in the medical domain [18]. As a result, patients may receive unreliable responses, dwarfing trust in CADs and thereby hindering the practical use of such systems in real medical scenarios.

In order to tackle the challenges mentioned above, we propose ChatCAD+ in this paper. And our contributions are made in the following aspects. **(1) Universal image interpretation.** Due to the difficulty in obtaining a unified CAD network tackling various images currently, ChatCAD+ incorporates a domain identification module to work with a variety of CAD

\* These authors contribute equally.

Zihao Zhao, Jinchen Gu, Yitao Zhu, Lanzhu Mei, and Zhiming Cui are with the School of Biomedical Engineering, ShanghaiTech University, Shanghai 201210, China (email: {zihaozhao10, cuizm.neu.edu}@gmail.com, {gujch12022,zhuYT, meilzhj}@shanghaitech.edu.cn)

Sheng Wang and Zixu Zhuang are with the School of Biomedical Engineering, Shanghai Jiao Tong University, Shanghai 200030, China, Shanghai United Imaging Intelligence Co., Ltd., Shanghai 200230, China, and also ShanghaiTech University, Shanghai 201210, China. (e-mail: {wsheng, zixuzhuang}@sjtu.edu.cn)

Qian Wang and Dinggang Shen are with the School of Biomedical Engineering, ShanghaiTech University, Shanghai 201210, China, the Shanghai Clinical Research and Trial Center, Shanghai 201210, China. Dinggang Shen is also with Shanghai United Imaging Intelligence Co. Ltd., Shanghai 200230, China. (e-mail: {wangqian2, dgshen}@shanghaitech.edu.cn)

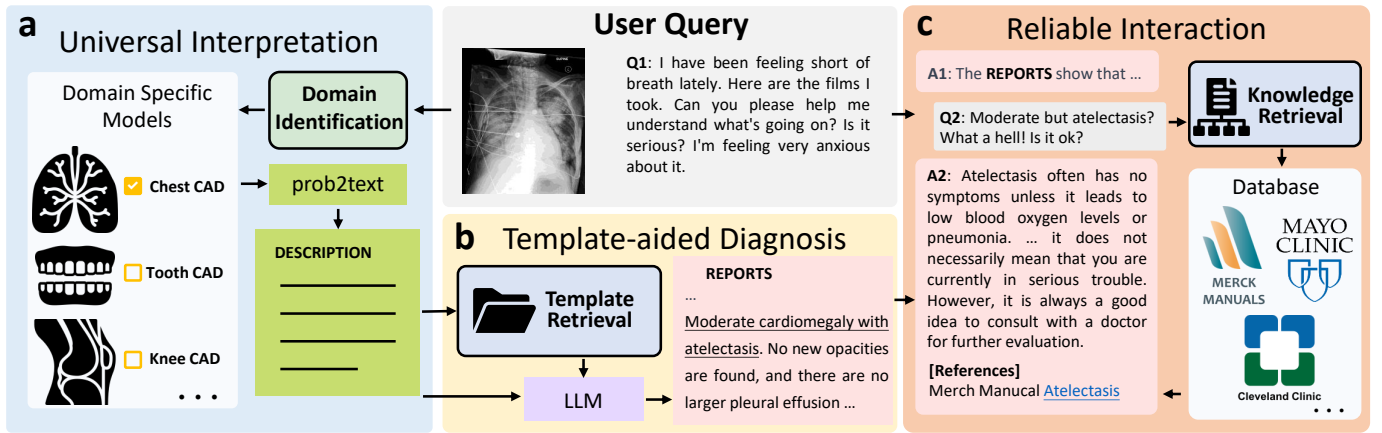


Fig. 1. Overview of the proposed ChatCAD+, which is composed of three key components. (a) Universal interpretation. This module automatically identifies the domain of the image query and selects the appropriate Computer Assisted Diagnosis (CAD) network(s) for image interpretation. The output is converted into medical text description for further processing. (b) Template-aided diagnosis. Several template reports are retrieved from the in-house dataset to instruct the writing of final diagnostic reports. (c) Reliable interaction. Given the text query, the Large Language Model (LLM) retrieves related knowledge from medical knowledge databases to provide reliable medical treatments and explanations.

models (c.f. Fig. 1(a)). ChatCAD+ can select a corresponding model given the input medical image. The tentative output of the CAD network is converted into text descriptions that reflect image features, making them applicable for diagnostic reporting subsequently. (2) **Template-aided diagnosis.** Top- $k$  reports that are related to the input image are retrieved from a clinic database via the proposed template retrieval system (c.f. Fig. 1(b)). The retrieved  $k$  report templates then serve as cues to guide the style of the LLM-generated report. (3) **Knowledge-based reliable interaction.** As illustrated in Fig. 1(c), ChatCAD+ does not directly provide medical advice. Instead, it first seeks help via our proposed knowledge retrieval module for relevant knowledge from professional sources, e.g. Merck Manuals, Mayo Clinic, and Cleveland Clinic. Then, the LLM considers the retrieved knowledge as a reference to provide reliable medical advice.

In summary, our ChatCAD+ for the first time builds a universal and reliable medical dialogue system primarily. The improved quality of answers and diagnostic reports of the chatbot reveals the potential of LLMs in interactive medical consultation.

## II. RELATED WORKS

### A. Large Language Models in Healthcare

Recent advances in Transformer architecture [21] and computing power have enabled the training of large language models with billions of parameters, leading to a significant improvement in their ability to summarize, translate, predict and generate human-like text [22]–[24]. In the pre-ChatGPT era, several healthcare language models have been developed based on general-purpose model weight and training schemes. BioBERT [25] and PubMedBERT [26] are examples of BERT [27] fine-tuned on PubMed, whereas ClinicalBERT [28] was further trained on the MIMIC-CXR dataset.

After ChatGPT showed great potential of 100B-scale models, researchers expand the healthcare language model to a

much larger scale and give very promising results. Med-PaLM [23] was developed in late 2022 using curated biomedical corpora and human feedback, and showed promising results, including a 67.6% accuracy on the MedQA exam. ChatGPT, which was not given supplementary medical training, still passed all three parts of the USMLE and achieved over 50% accuracy across all exams and surpassed 60% accuracy in the majority of them [29]. ChatCAD [14] combined medical image analysis models with ChatGPT and offered an interactive computer-aided diagnosis. ChatDoctor [17] was a medical chat model fine-tuned on LLaMA model using clinical QA that is synthesized by ChatGPT. DoctorGLM [18] demonstrated that finetuning an LLM for healthcare use could be done at an affordable cost.

### B. Multi-modality Large Models

Initially, end-to-end pretraining is a commonly employed technique for facilitating multi-modal input. Various model architectures have been suggested, including the dual-encoder structure of CLIP [30], encoder-decoder architecture Pali [31] and unified transformer architecture BEiT [32]. These methods employ large-scale image-text datasets for comprehensive pretraining. However, as model sizes grow, the computational expense of pretraining can become prohibitively high.

To reduce training costs, researchers have started utilizing pre-existing pretrained models. Frozen [33] fine-tuned an image encoder, whose outputs served as soft prompts for the language model. Flamingo [34] introduced cross-attention layers into the LLM to incorporate visual features, pre-training these new layers on billions of image-text pairs. BLIP-2 [35] leveraged both frozen image encoders and frozen LLMs to achieve stronger performance at a lower computation cost.

In more recent studies, researchers have opted not to train anything, but instead design prompts that allow LLMs to utilize vision models. For example, Visual-ChatGPT [36] connected ChatGPT and a series of visual foundation models to enable sending and receiving images during chatting. ChatCAD [14] linked existing CAD models with LLMs to boost

diagnostic accuracy and enhance patient care. Grounded-SAM combined a trained Grounding DINO model [37] and a trained SAM model [38] to detect and segment natural image objects with text inputs.

### III. METHOD

The proposed ChatCAD+ is a multi-modality system, which handles both image and text. Note that, in this paper, the term *modality* follows the definition of language plus image, which is somehow different from the often-used concept of medical image modality. As the input image is not restricted to a fixed image domain, it passes through universal interpretation, and the result is forwarded to template-aided diagnosis to get the report for the user. The text query is processed through the knowledge retrieval module, which retrieves clinically-sound knowledge to support the LLM.

#### A. Universal Interpretation

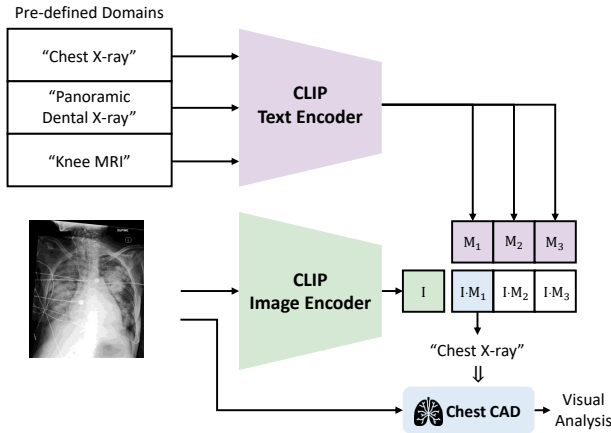


**Fig. 2. The illustration of domain identification.** Cosine similarity will be computed between the input image and each pre-defined text phrase, and the text with the highest score is determined to represent the image domain. The corresponding CAD model is hence called to perform interpretation.

The process of universal interpretation can be divided into three steps. Initially, the proposed domain identification module is employed to determine the specific domain of the medical image. Subsequently, the corresponding domain-specific model is activated to interpret the image. Finally, the result of the interpretation is converted into a text description via the rule-based prob2text module for further processing.

Identifying the domain of a medical image is a crucial step for the subsequent operations of ChatCAD+. To achieve this, we employ a method of visual-language contrast that computes the cosine similarity between the input image and textual representations of various potential domains. This approach takes advantage of language's ability to densely describe the features of a particular type of image and its ease of extensibility. In particular, we employ the pre-trained CLIP model [30] to encode both the medical image and the text associated with domains of interest. In this study, we demonstrate upon three domains: Chest X-ray, Panoramic Dental X-ray, and Knee MRI. The workflow is depicted in Fig. 2. Assuming

there are three domains  $D_1, D_2, D_3$ , along with their textual representations  $M_1, M_2, M_3$ , and also a visual representation denoted as  $I$  for the input image, the process is defined as follows

$$D_{\text{pred}} = \operatorname{argmax}_{i \in \{1,2,3\}} \frac{I \cdot M_i}{\|I\| \|M_i\|}, \quad (1)$$

where  $D_{\text{pred}}$  denotes the prediction of the medical image domain. The module thereby calls the domain-specific CAD model to analyze visual information given  $D_{\text{pred}}$ .

The gap between the CAD models for images and the following LLM is bridged by converting the output of CAD into text. For example, an image diagnosis model typically outputs tensors representing the likelihood of certain clinical findings. To establish a link between image and text, these tensors are transformed into textual descriptions according to diagnostic-related rules, which is denoted as **prob2text** in Fig. 1(a).

TABLE I

THE ILLUSTRATION OF PROB2TEXT. P3 IS THE DEFAULT SETTING.

CAD Model $\rightarrow$ (disease: prob)	
P1 (direct)	"{disease} score: {prob}"
P2 (simplistic)	<b>prob</b> $\in[0, 0.5]$ : "No Finding" <b>prob</b> $\in[0.5, 1]$ : "The prediction is {disease}"
P3 (illustrative)	<b>prob</b> $\in[0, 0.2]$ : "No sign of {disease}" <b>prob</b> $\in[0.2, 0.5]$ : "Small possibility of {disease}" <b>prob</b> $\in[0.5, 0.9]$ : "Patient is likely to have {disease}" <b>prob</b> $\in[0.9, 1]$ : "Definitely have {disease}"

The prob2text tool has been designed with the goal of presenting clinically relevant information in a manner that is more easily interpretable by LLMs. The details of the prompt design are illustrated in Table I. Using Chest X-ray as an example, we follow the three types (P1-P3) of prompt designs in [14] and adopt **P3 (illustrative)** as the recommended setting in this study. Concretely, it employs a grading system that maps the numerical scores into clinically illustrative descriptions of disease severity. The scores are divided into four levels based on their magnitude: "No sign", "Small possibility", "Likely", and "Definitely". The corresponding texts are then used to describe the likelihood of different observations in Chest X-ray, providing a concise and informative summary of the patient's condition. The prompt design for Panoramic Dental X-ray and Knee MRI are in similar ways. And other prompt designs, such as P1 and P2 [14], will be discussed in a later section.

#### B. Template-aided Diagnosis

The LLM utilizes a text description to generate a diagnostic report based on visual characteristics. This process is facilitated through prompts like "Write a report based on results from Network(s)". It is important to note that, when applicable, an additional report generation network is commonly integrated for each identified image domain. This integration allows the LLM to combine the generated reports from different networks, leading to an overall enhancement of the report.

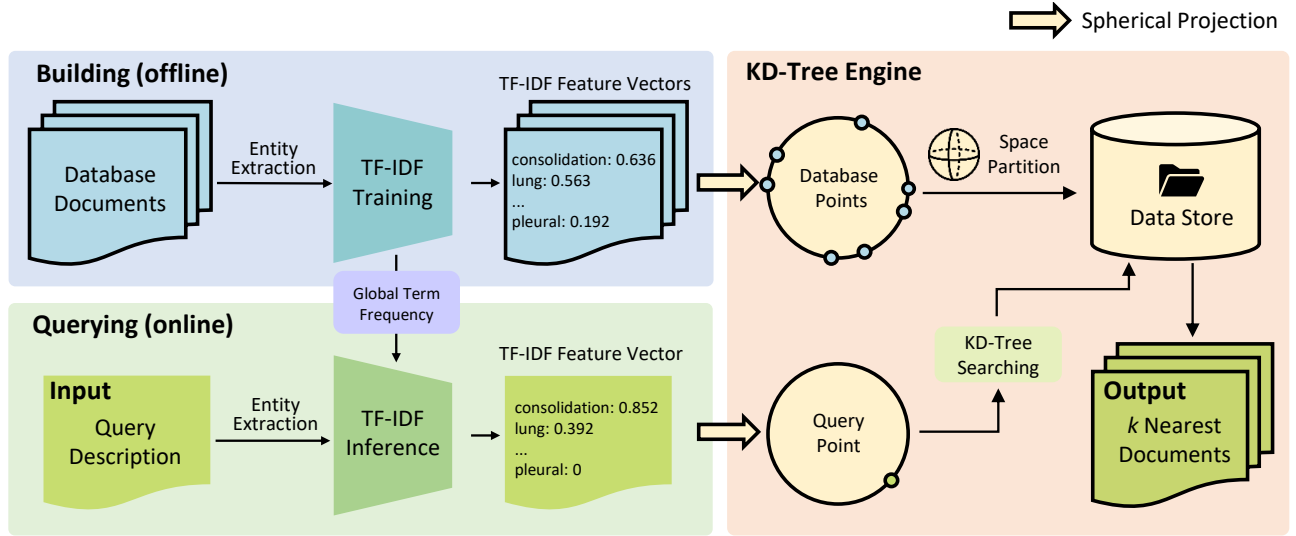


**Fig. 3. Template retrieval system.** The system performs online querying by leveraging the global term frequency learned during training to infer the TF-IDF score of the query description. All data points, during training and querying, are projected onto the surface of a unit ball, so that KD-Tree engine can swiftly retrieves a ranked list of the top  $k$  text documents that exhibit the highest similarity to the query features.

Such paradigm has been studied in [14], wherein they noted that ChatGPT exhibits a distinct writing style that sets it apart from human experts. This distinction is a crucial aspect to consider when developing a professional diagnosis system. To address this concern, we offer top- $k$  reports that share similar semantics with the text description from the report database via a template retrieval system, to guide the LLM in refining its writing style.

The proposed template retrieval system models each report in a database into the following TF-IDF features. It further adopts KD-Tree data structure to speed up the process of retrieval. The process is depicted in Fig. 3. For simplification, we take MIMIC-CXR as an example in this section. The retrieval system is built on the training set of the MIMIC-CXR dataset, with  $N$  denoting its size. Specifically, the TF-IDF score of a term  $t$  in a document  $d$  is computed as

$$\text{TF-IDF}(t, d) = \text{TF}(t, d) \cdot \text{IDF}(t), \quad (2)$$

where  $\text{TF}(t, d)$  represents the frequency of the term  $t$  appearing in the document  $d$ , and  $\text{IDF}(t)$  (inverse document frequency) quantifies the rarity or commonness of  $t$  across all documents. In particular, we determine  $\text{IDF}(t)$  by  $n_t$ , which denotes the number of documents containing  $t$ , following:

$$\text{IDF}(t) = -\log \frac{n_t}{N}. \quad (3)$$

To improve the specificity of disease-related information, we select 17 medical entities of thoracic diseases annotated in MIMIC-CXR as the dictionary of terms. We then compute the TF-IDF feature of each document in the MIMIC-CXR dataset, which combines the TF-IDF scores for every term in the dictionary.

After calculating the TF-IDF features of each document  $d$ , we organize all documents in KD-Tree [39], which enables fast online querying. KD-Tree is a space-partitioning data structure used for organizing data in a high-dimensional space.

It can implement  $k$ -nearest-neighbor querying in  $O(\log(n))$  time on average. Since the classical KD-Tree works with  $L_2$  distance, we transform the similarity metric to the  $L_2$  distance by projecting all TF-IDF feature vectors of documents onto the surface of a unit hypersphere, as demonstrated in the right panel of Fig. 3. This allows for the efficient use of the KD-Tree structure to perform similarity queries. We observe that the cosine similarity between two vectors monotonically decreases as the angle between them increases. At the same time, after mapping each vector onto the surface of a unit hypersphere, their  $L_2$  distance monotonically increases with the angle between them. This relationship can be formally proved as follows:

$$\begin{aligned} \cos(\vec{q}, \vec{v}) &= \cos\left(\frac{\vec{q}}{|\vec{q}|}, \frac{\vec{v}}{|\vec{v}|}\right) = \cos(\theta), \\ L_2\left(\frac{\vec{q}}{|\vec{q}|}, \frac{\vec{v}}{|\vec{v}|}\right) &= 2r \cdot \sin\left(\frac{\theta}{2}\right). \end{aligned} \quad (4)$$

Here,  $\vec{q}$  is the feature vector of the query,  $\vec{v}$  is the feature vector of a sample in the database,  $r$  is the radius of the hypersphere (here equals 1),  $\theta$  is the angle between  $\frac{\vec{q}}{|\vec{q}|}$  and  $\frac{\vec{v}}{|\vec{v}|}$ , and  $\theta \in [0, \pi]$ . Therefore, for any vector  $\vec{q}$  as query and two vector  $\vec{v}_i$  and  $\vec{v}_j$  in database,  $\cos(\vec{q}, \vec{v}_i) > \cos(\vec{q}, \vec{v}_j) \Leftrightarrow \theta_i < \theta_j \Leftrightarrow L_2\left(\frac{\vec{q}}{|\vec{q}|}, \frac{\vec{v}_i}{|\vec{v}_i|}\right) < L_2\left(\frac{\vec{q}}{|\vec{q}|}, \frac{\vec{v}_j}{|\vec{v}_j|}\right)$ . Since we only care about the rank of cosine similarity, we can convert every  $\vec{q}$  and  $\vec{v}_i$  to  $\frac{\vec{q}}{|\vec{q}|}$  and  $\frac{\vec{v}_i}{|\vec{v}_i|}$ , and then use  $L_2$  metric for querying. After the projection, the rank remains unchanged, and thus KD-Tree can be utilized for efficient querying.

The querying is performed online as demonstrated at the bottom of Fig. 3. The global term frequency, which represents the frequency of a term throughout the entire training set, is utilized for the inference of the TF-IDF feature of the query description. Once the feature is obtained, the KD-Tree engine efficiently returns a list of  $k$  (we set  $k=3$  by default) text documents that share the most similar features with the query.



After obtaining  $k$  reports as templates, the LLM is asked to write the report on the basis of CAD network(s) while following the writing style of templates. The improvement is illustrated in Section IV.

### C. Reliable Interaction

The proposed ChatCAD+ offers reliable medical advice via the construction of a professional knowledge database and LLM-based knowledge retrieval. In this study, we demonstrate using the Merck Manuals. The Merck Manuals are a series of healthcare reference books that provide evidence-based information on the diagnosis and treatment of diseases and medical conditions.

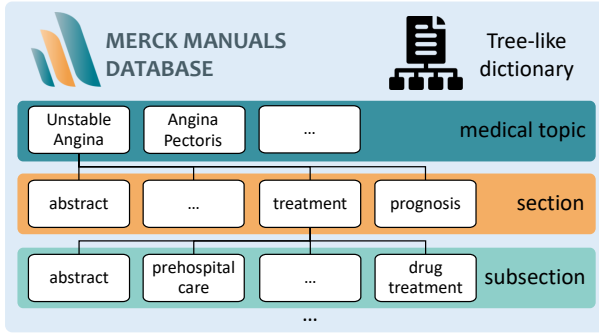


Fig. 4. The illustration of the hierarchical Merck Manuals database.

The implementation of LLM-based knowledge retrieval leverages the Chain-of-Thought (CoT) technique, which is widely known for its ability to enhance the performance of LLM in problem-solving. CoT breaks down a problem into a series of sub-problems and then synthesizes the answers to these sub-problems progressively to solve the original problem. Humans typically do not read the entire knowledge base but rather skim through topic titles to find what they are looking for. Taking inspiration from this approach, we have designed a prompt system that automatically guides the LLM to execute such searches. Correspondingly, we have structured the Merck Manuals database as a hierarchical dictionary, with topic titles of different levels serving as keys, as shown in Fig 4.

The proposed knowledge retrieval methods operates as follows in Algorithm 1. Initially, we provide the LLM with only titles of five related medical topics in the database, and then allow the LLM to select the most relevant topic. Once the LLM has made its choice, we provide it with the relevant medical knowledge pertaining to that topic. If the topic has multiple sections, we provide the LLM with both medical knowledge and a list of sections, and repeat this process. The LLM may return to the parent topic if it determines that none of the provided topics are relevant to the query. The system continues until the LLM has identified relevant medical knowledge, and at this time it is prompted to display relevant information and the system terminates.

## IV. EXPERIMENTAL RESULTS

### Algorithm 1: LLM-based knowledge retrieval

```

# infobase: Tree-like dictionary
# info_stack: A stack store history information
# query: User's text input
# bot: A LLM-based chatbot
# prompt(): Present topics to be selected

all_topics=list(infobase.keys())
# topics of interest
related_topics=kNN(query,all_topics)
info_stack.push(related_topics)
response=bot.get_needed_topic(related_topics)
while True:
    # terminate
    if response == "found":
        found_knowledge=bot.get_info()
        return found_knowledge
    # backtrack
    elif response == "no choice":
        info_stack.pop()
        next_item_dict=info_stack.top()
    # select a valid topic
    elif response in related_topics:
        this_item_dict=info_stack.top()
        next_item_dict=this_item_dict[response]
        info_stack.push(next_item_dict)
        related_topics=prompt(next_item_dict)
        response=bot.get_needed_topic(related_topics)

```

### A. Dataset and Implementations

For a fair comparison, the performance of ChatCAD+ is assessed on the public MIMIC-CXR dataset [40] and two private datasets. The MIMIC-CXR is a large public dataset of Chest X-ray images, associated radiology reports, and other clinical data. The dataset consists of 377,110 de-identified Chest X-ray images and associated 227,827 radiology reports. The MIMIC-CXR dataset allows us to measure the quality of diagnostic accuracy and report generation, as most report generation methods are designed specifically for Chest X-ray.

The second dataset of Dental X-ray consists of 426 panoramic X-ray images that were collected from real-world clinics. The size of the image is  $2903 \times 1536$ . Each patient has corresponding clinical records of golden standard, measured and diagnosed by experienced experts.

The third dataset of Knee MRI is a collection of images obtained from patients who visited Shanghai Sixth People's Hospital affiliated with Shanghai Jiao Tong University School of Medicine. The dataset consists of 1205 images captured using a Philips Achieva 3.0T TX MRI scanner. The imaging protocol used a T2-weighted sequence with fat suppression and fast spin echoes to acquire the images.

**Domain Specific CAD Models.** For Chest CAD, the thoracic disease classifier [41] is pre-trained on the official training split of the CheXpert [42] dataset, with over 224k Chest X-rays. At the same time, the Chest X-ray report generation network [12] adopted in templated-aided diagnosis is pre-trained on the training split of MIMIC-CXR. The periodontal diagnosis model proposed in [43] is utilized as Tooth CAD. For Knee CAD, we adopt the model proposed in [9]. During implementation, both pre-trained models were kept frozen.

**Evaluations.** ChatGPT was adopted as the default LLM

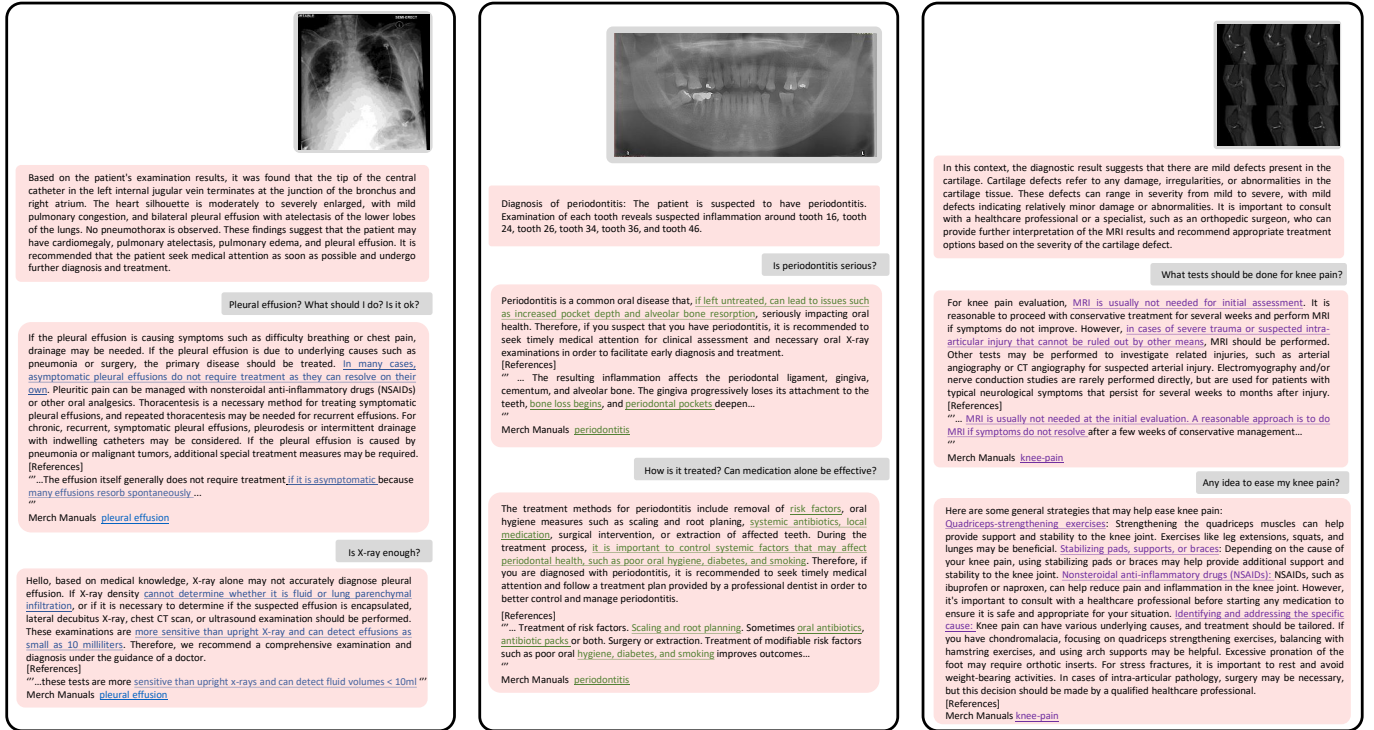


Fig. 5. Examples of universal and interactive medical consultation using ChatCAD+, with ChatGPT as the default LLM. The underlined text signifies information obtained from reputable medical websites, which is not comprehensively incorporated in ChatGPT.

in all experiments. The quality of LLM-aided diagnosis was tested on the official test set of the MIMIC-CXR dataset, focusing on five findings (cardiomegaly, edema, consolidation, atelectasis, and pleural effusion). Due to limitations on the per-hour accesses of OpenAI API-Key, we randomly selected 200 samples for each finding of interest, resulting in a total of 1000 test samples. To evaluate the performance of LLM-aided diagnosis, we used several widely-used Natural Language Generation (NLG) metrics, including BLEU [44], METEOR [45], and ROUGE-L [46]. Specifically, BLEU measures the similarity between generated and ground-truth reports by counting word overlap, whereas METEOR considers synonym substitution and evaluates performance on both sentence level and report level. Meanwhile, ROUGE-L evaluates based on the length of the longest common subsequence. We also measured three classification metrics, including precision (PR), recall (RC), and F1-score (F1), on the 1000 test samples. These metrics provide additional insight into the performance of LLM-aided diagnosis. If not specified, we choose P3 as the default prompt design in LLM-aided diagnosis and  $k=3$  for template retrieval. Note that we adopt Chexbert labeler [47] to extract labels from generated reports, and calculate classification metrics on them.

## B. Universal and Reliable CAD

Fig. 5 demonstrates the universal application and reliability of our proposed method. The ChatCAD+ can process different medical images and provide proper diagnostic reports. Users can interact with ChatCAD+ and ask additional questions for further clarification.

By leveraging external medical knowledge, the enhanced ChatCAD+ is capable of delivering medical advice in a more professional manner. In Fig. 5, each reply from ChatCAD+ includes a reference, and the pertinent knowledge obtained from the external database is underlined for emphasis. For instance, in the scenario where the question is raised about whether a Chest X-ray is sufficient for diagnosing pleural effusion, ChatGPT would simply recommend a CT scan without providing a convincing explanation. In contrast, ChatCAD+ is capable of informing the patient that CT scans have the capability to detect effusions as small as 10 milliliters, thereby providing a more detailed and informative response.

The effectiveness of our proposed knowledge retrieval method is qualitatively compared. Existing knowledge retrieval methods tend to follow the paradigm of LangChain [48], which involves dividing the text into paragraphs and then utilizing sentence transformers to compare the similarity between the embedding of a user query and all paragraphs. This kind of knowledge retrieval method can hardly handle the professional medical knowledge database. We select the retrieval method adopted in [48] as the baseline and compare its performance with our proposed method in Table IV and Table V on the Merck Manuals. The results clearly illustrate the advancement of our method. On the contrary, [48] struggles to identify relevant medical topics due to limited vocabulary size. This issue can be worse if the question of the user does not explicitly point to any medical topics or involve multiple medical entities.

TABLE II

DIAGNOSTIC ACCURACY COMPARISON WITH DIFFERENT METHODS (**BOLD BLACK**: THE BEST METHOD. **BOLD PURPLE**: THE SECOND BEST.)

Methods		Cardiomegaly	Edema	Consolidation	Atelectasis	Pleural Effusion	Average
R2GenCMN [12]	PR	<b>0.649</b>	0.600	<b>0.419</b>	<b>0.499</b>	<b>0.848</b>	<b>0.603</b>
	RC	0.507	0.286	0.051	0.448	0.406	0.339
	F1	0.569	0.387	0.091	0.472	0.549	0.414
VLCI [13]	PR	0.571	<b>0.813</b>	<b>0.439</b>	<b>0.519</b>	<b>0.841</b>	<b>0.636</b>
	RC	0.352	0.060	0.070	0.312	0.421	0.243
	F1	0.435	0.113	0.121	0.389	0.561	0.324
ChatCAD	PR	0.581	0.558	0.289	0.451	0.753	0.526
	RC	<b>0.742</b>	<b>0.472</b>	<b>0.441</b>	<b>0.688</b>	<b>0.672</b>	<b>0.603</b>
	F1	<b>0.652</b>	<b>0.511</b>	<b>0.349</b>	<b>0.545</b>	<b>0.710</b>	<b>0.553</b>
ChatCAD+	PR	<b>0.605</b>	<b>0.604</b>	0.264	0.498	0.834	0.561
	RC	<b>0.624</b>	<b>0.323</b>	<b>0.129</b>	<b>0.552</b>	<b>0.517</b>	<b>0.429</b>
	F1	<b>0.614</b>	<b>0.421</b>	<b>0.173</b>	<b>0.524</b>	<b>0.638</b>	<b>0.474</b>

TABLE III

COMPARATIVE RESULTS WITH PREVIOUS STUDIES AND DIFFERENT PROMPT SETTINGS. THE BEST VALUES ARE HIGHLIGHTED IN BOLD BLACK, WHILE THE SECOND-BEST VALUES ARE MARKED IN BOLD PURPLE. THE DEFAULT SETTING IS CHATCAD+ (P3).

Model	BLEU-1	BLEU-2	BLEU-3	BLEU-4	Corpus BLEU	METEOR	ROUGE-L
R2GenCMN	<b>0.367</b>	<b>0.083</b>	<b>0.027</b>	<b>0.012</b>	0.035	0.210	<b>0.183</b>
ChatCAD (P3)	0.285	0.064	0.017	0.006	0.036	0.233	0.168
ChatCAD+ (P1)	0.303	0.069	0.019	0.007	0.041	0.227	0.168
ChatCAD+ (P2)	0.313	0.074	0.021	0.008	<b>0.044</b>	<b>0.233</b>	0.173
ChatCAD+ (P3)	<b>0.316</b>	<b>0.076</b>	<b>0.021</b>	<b>0.008</b>	<b>0.044</b>	<b>0.241</b>	<b>0.174</b>

### C. Quality of the Template-aided Diagnosis

The diagnostic accuracy of different methods was compared and presented in Table II, with R2GenCMN [12] being the selected report generation network in template-aided diagnosis, and VLCI [13] being the state-of-the-art method. Notably, ChatCAD+ demonstrated superior performance in terms of RC and F1 when compared to R2GenCMN, suggesting higher accuracy and better information retrieval ability. Generally, ChatCAD+ was the second-best overall method based on average performance across all diseases of interest, as indicated by bold purple highlighting in Table II. However, it should be noted that ChatCAD+ exhibited inferior classification performance compared to ChatCAD. It seems that the introduction of template retrieval has a negative impact. However, we will demonstrate later that this degradation is a substitute for better natural language generation methods.

In Table III, the quality of language generation is assessed using various NLG metrics. ChatCAD+ demonstrates a substantial advantage over ChatCAD across all NLG metrics, as observed in the results obtained using P3. Compared with R2GenCMN, which imitates the human language style well while weak in diagnostic accuracy, ChatCAD+ also shows better performance on METEOR and Corpus BLEU, indicating that ChatCAD+ possesses both proficient report generation and diagnostic capability without favoring either.

Additionally, the impact of prompt designs is investigated. It is observed that the style of clinical text descriptions does not significantly affect most metrics, except for METEOR [49], where P3 achieves the highest METEOR score and P1 obtains the lowest. This phenomenon may be attributed to the similarity of P3 to human language style, as it reflects the severity

of the disease using rhetoric, whereas P1 directly displays the probability without extensive post-process. ChatCAD+ shows a significant advantage over ChatCAD on all NLG metrics using P3, which underscores the rationality of utilizing template reports as exemplars.

### D. Ablation Study

In this subsection, we conduct an empirical study on the impact of template retrieval, which serves as a crucial component in enhancing the quality of report generation.

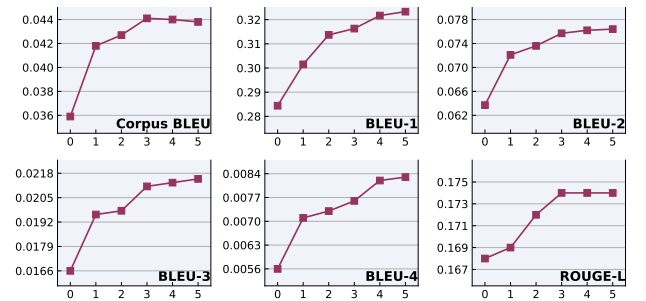


Fig. 6. Ablation study on the MIMIC-CXR dataset w.r.t. the number of retrieved templates. A range of values, varying from 0 to 5, was chosen for  $k$ , and its influence is evaluated on several NLG metrics.

**Importance of template guidance.** In Fig. 6, we compare the NLG performance with different numbers of retrieved templates. As  $k$  increases, the overall performance shows an upward trend. Moreover, in most cases, the largest improvement in performance occurs when  $k$  changes from 0 to 1. This indicates that regardless of the quantity, as long as templates

are provided as references, the quality of generated reports can be significantly enhanced. Meanwhile, the performance improvement tends to saturate around  $k=3$ , and further increasing  $k$  does not result in more significant improvements, which validates the rationality of the adopted default setting.

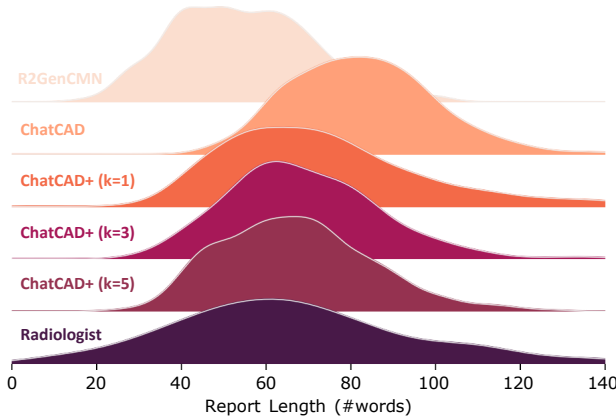


Fig. 7. Distributions of report length when changing  $k$ .

**Influence on report length distribution.** The distribution of report length is demonstrated in Fig. 7 by varying the value of  $k$ . Report length serves as an important criterion [50] to measure the similarity to ground truth radiology reports. A straightforward observation is that the distribution of ChatCAD exhibits a significant shift from that of the radiologist. In contrast, ChatCAD+ shows a more fitted curve irrespective of the value of  $k$ .

## V. LIMITATIONS AND DISCUSSION

In this work, we have developed ChatCAD+, a universal and reliable interactive CAD system that can accept images of different domains as valid input. We expect that the proposed paradigm of universal CAD networks can motivate the advancement of cross-domain model literature in medical image domain. Furthermore, the template retrieval system enhances the report generation ability of ChatCAD+ and let it act more like a radiologist. The LLM-based knowledge retrieval method enables the LLM to search by itself, and utilize the external medical knowledge database to provide convincing medical treatments. In this way, our ChatCAD+ has utilized the Merck Manuals database as its primary external knowledge database, which may be considered limited in its scope. However, we are confident in the versatility of our proposed LLM-based knowledge retrieval method, as it can be readily adapted to incorporate other databases. By doing so, we anticipate that the reliability of ChatCAD+ will be greatly enhanced. There are several limitations that must be acknowledged in this study. While we have succeeded in enhancing the report generation capacity of our model to closely resemble that of a radiologist, it has come at the cost of reduced diagnostic accuracy.

Additionally, the knowledge retrieval method we employed is relatively slow, as its efficacy is closely tied to the response speed of the OpenAI API. These limitations provide an opportunity for future research to address them and improve upon the current findings.

## REFERENCES

- [1] OpenAI. (2023) Chatgpt: Optimizing language models for dialogue. [Online]. Available: <https://openai.com/blog/chatgpt/> 1
- [2] H. Touvron, T. Lavril, G. Izacard, X. Martinet, M.-A. Lachaux, T. Lacroix, B. Rozière, N. Goyal, E. Hambro, F. Azhar, A. Rodriguez, A. Joulin, E. Grave, and G. Lample, “Llama: Open and efficient foundation language models,” *arXiv preprint arXiv:2302.13971*, 2023. 1
- [3] O.-A. Contributors, “Open-Assistant,” <https://github.com/LAION-AI/Open-Assistant>, 2023. 1
- [4] J. Qiu, L. Li, J. Sun, J. Peng, P. Shi, R. Zhang, Y. Dong, K. Lam, F. P.-W. Lo, B. Xiao *et al.*, “Large ai models in health informatics: Applications, challenges, and the future,” *arXiv preprint arXiv:2303.11568*, 2023. 1
- [5] Y. Huang, A. Gomaa, T. Weissmann, J. Grigo, H. B. Tkhatyat, B. Frey, U. S. Gaip, L. V. Distel, A. Maier, R. Fietkau *et al.*, “Benchmarking chatgpt-4 on acr radiation oncology in-training exam (txit): Potentials and challenges for ai-assisted medical education and decision making in radiation oncology,” *arXiv preprint arXiv:2304.11957*, 2023. 1
- [6] J. Holmes, Z. Liu, L. Zhang, Y. Ding, T. T. Sio, L. A. McGee, J. B. Ashman, X. Li, T. Liu, J. Shen *et al.*, “Evaluating large language models on a highly-specialized topic, radiation oncology physics,” *arXiv preprint arXiv:2304.01938*, 2023. 1
- [7] S. Biswas, “Chatgpt and the future of medical writing,” p. e223312, 2023. 1
- [8] V. W. Xue, P. Lei, and W. C. Cho, “The potential impact of chatgpt in clinical and translational medicine,” *Clinical and Translational Medicine*, vol. 13, no. 3, 2023. 1
- [9] Z. Zhuang, L. Si, S. Wang, K. Xuan, X. Ouyang, Y. Zhan, Z. Xue, L. Zhang, D. Shen, W. Yao *et al.*, “Knee cartilage defect assessment by graph representation and surface convolution,” *IEEE Transactions on Medical Imaging*, 2022. 1, 5
- [10] Z. Cui, Y. Fang, L. Mei, B. Zhang, B. Yu, J. Liu, C. Jiang, Y. Sun, L. Ma, J. Huang *et al.*, “A fully automatic ai system for tooth and alveolar bone segmentation from cone-beam ct images,” *Nature communications*, vol. 13, no. 1, p. 2096, 2022. 1
- [11] S. Wang, X. Ouyang, T. Liu, Q. Wang, and D. Shen, “Follow my eye: Using gaze to supervise computer-aided diagnosis,” *IEEE Transactions on Medical Imaging*, 2022. 1
- [12] Z. Chen, Y. Shen, Y. Song, and X. Wan, “Generating radiology reports via memory-driven transformer,” in *Proceedings of the Joint Conference of the 59th Annual Meeting of the Association for Computational Linguistics and the 11th International Joint Conference on Natural Language Processing*, Aug. 2021. 1, 5, 7
- [13] W. Chen, Y. Liu, C. Wang, G. Li, J. Zhu, and L. Lin, “Visual-linguistic causal intervention for radiology report generation,” *arXiv preprint arXiv:2303.09117*, 2023. 1, 7
- [14] S. Wang, Z. Zhao, X. Ouyang, Q. Wang, and D. Shen, “Chatcad: Interactive computer-aided diagnosis on medical image using large language models,” *arXiv preprint arXiv:2302.07257*, 2023. 1, 2, 3, 4
- [15] L. Milecki, V. Kalogeiton, S. Bodard, D. Anglicheau, J.-M. Correas, M.-O. Timsit, and M. Vakalopoulou, “Medimp: Medical images and prompts for renal transplant representation learning,” *arXiv preprint arXiv:2303.12445*, 2023. 1
- [16] C. Niu and G. Wang, “Ct multi-task learning with a large image-text (lit) model,” *bioRxiv*, pp. 2023–04, 2023. 1
- [17] L. Yunxiang, L. Zihan, Z. Kai, D. Ruilong, and Z. You, “Chatdoctor: A medical chat model fine-tuned on llama model using medical domain knowledge,” *arXiv preprint arXiv:2303.14070*, 2023. 1, 2
- [18] H. Xiong, S. Wang, Y. Zhu, Z. Zhao, Y. Liu, Q. Wang, and D. Shen, “Doctorglm: Fine-tuning your chinese doctor is not a herculean task,” *arXiv preprint arXiv:2304.01097*, 2023. 1, 2
- [19] H. Wang, C. Liu, N. Xi, Z. Qiang, S. Zhao, B. Qin, and T. Liu, “Huatuo: Tuning llama model with chinese medical knowledge,” *arXiv preprint arXiv:2304.06975*, 2023. 1
- [20] B. Keno K., H. Tianyu, and C. Shan, “medalpaca: Finetuned large language models for medical question answering,” <https://github.com/kbressem/medAlpaca>, 2023. 1
- [21] A. Vaswani, N. Shazeer, N. Parmar, J. Uszkoreit, L. Jones, A. N. Gomez, E. Kaiser, and I. Polosukhin, “Attention is all you need,” in *Advances in neural information processing systems*, 2017, pp. 5998–6008. 2
- [22] T. Brown, B. Mann, N. Ryder, M. Subbiah, J. D. Kaplan, P. Dhariwal, A. Neelakantan, P. Shyam, G. Sastry, A. Askell *et al.*, “Language models are few-shot learners,” *Advances in neural information processing systems*, vol. 33, pp. 1877–1901, 2020. 2



<b>Q1</b> How to treat periodontitis? Is taking medication enough?
<b>K1 (Baseline)</b> Esophageal cancer can occur at a young age. Unna-Thost disease and Verner disease: autosomal dominant inheritance. Papillon-Lefèvre syndrome: autosomal recessive inheritance, onset within 6 months after birth. Severe periodontitis can lead to tooth loss. Vohwinkel syndrome: autosomal dominant inheritance, patients may experience progressive toe and finger amputation and high-frequency hearing loss. Diffuse non-epidermolytic palmoplantar keratoderma: this autosomal dominant inherited form develops in infancy, causing a sharply defined symmetric keratoderma affecting the entire palm and sole. Treatment: Symptomatic treatment includes the use of emollients, keratolytic agents, and physical methods for removal.
<b>K1 (Ours)</b> Treatment of risk factors Scaling and root planing Sometimes oral antibiotics, antibiotic packs, or both Surgery or extraction Treatment of modifiable risk factors such as poor oral hygiene, diabetes, and smoking improves outcomes.
... If deeper pockets persist, systemic antibiotics can be used. A common regimen is amoxicillin 500 mg orally 3 times a day for 10 days. In addition, a gel containing doxycycline or microspheres of minocycline can be placed into isolated recalcitrant pockets. These drugs are resorbed in 2 weeks. Another approach is to surgically eliminate the pocket and recontour the bone (pocket reduction/elimination surgery) so that the patient can clean the depth of the normal crevice (sulcus) between the tooth and gingiva. In certain patients, regenerative surgery and bone grafting are done to encourage alveolar bone growth. Splinting of loose teeth and selective reshaping of tooth surfaces to eliminate traumatic occlusion may be necessary. Extractions are often necessary in advanced disease. Contributing systemic factors should be controlled before initiating periodontal therapy. Ninety percent of patients with necrotizing ulcerative periodontitis due to HIV (HIV-associated periodontitis) respond to combined treatment with scaling and planing, irrigation of the sulcus with povidone-iodine (which the dentist applies with a syringe), regular use of chlorhexidine mouth rinses, and systemic antibiotics, usually metronidazole 250 mg orally 3 times a day for 14 days. Localized aggressive periodontitis requires periodontal surgery plus oral antibiotics (eg, amoxicillin 500 mg 4 times a day or metronidazole 250 mg 3 times a day for 14 days).
<b>A1 (Ours)</b> The treatment of periodontitis requires a comprehensive approach that considers risk factors, scaling and root planing, oral antibiotics, and local medications. For all cases of periodontitis, the first stage of treatment involves thorough cleaning, scaling and root planing, and reinforcement of daily oral hygiene. If deep periodontal pockets are present, systemic antibiotics may be used, with amoxicillin 500mg orally, three times a day for 10 days being a commonly used method. The second stage of treatment involves surgical removal of periodontal pockets and bone reshaping to allow the patient to self-clean the base of the gingival sulcus. Localized aggressive periodontitis requires periodontal surgery in combination with oral antibiotics. At the same time, systemic factors such as poor oral hygiene, diabetes, and smoking must be controlled to improve the prognosis. Therefore, drug therapy alone is not sufficient and comprehensive treatment is necessary.
<b>Q2</b> What tests should be done for knee pain?
<b>K2 (Baseline)</b> Patellar tendon tear: the patella is palpable and displaced upwards (high-riding patella). Transverse patellar fracture: a gap between the two pieces of the patella may be palpable. However, due to significant local swelling, these symptoms may be mistaken for knee ligament injury with joint effusion. If a patient presents with knee swelling and pain after injury, the clinician will ask the patient to sit down and attempt to extend the injured leg to test knee extension actively or lie flat and elevate the injured leg. After knee swelling following trauma, remember to test the knee's ability for independent extension. Routine knee joint X-ray examination should be performed. Knee X-rays can show a high or low position of the patella. X-rays can reveal dislocation or patellar fractures, but they may also appear normal.
<b>K2 (Ours)</b> MRI is usually not needed at the initial evaluation. A reasonable approach is to do MRI if symptoms do not resolve after a few weeks of conservative management. However, MRI is often done when severe injury or significant intra-articular injury is suspected or cannot be otherwise excluded. Other tests may be done to check for related injuries: Arteriography or CT angiography to check for suspected arterial injuries Electromyography and/or nerve conduction studies, which are rarely done immediately but more typically done when nerve symptoms persist weeks to months after the injury.
<b>A2 (Ours)</b> For knee pain evaluation, MRI is usually not needed for initial assessment. It is reasonable to proceed with conservative treatment for several weeks and perform MRI if symptoms do not improve. However, in cases of severe trauma or suspected intra-articular injury that cannot be ruled out by other means, MRI should be performed. Other tests may be performed to investigate related injuries, such as arterial angiography or CT angiography for suspected arterial injury. Electromyography and/or nerve conduction studies are rarely performed directly, but are used for patients with typical neurological symptoms that persist for several weeks to months after injury. Therefore, which tests are needed depends on the specific situation of the patient.

TABLE IV

COMPARISON BETWEEN KNOWLEDGE RETRIEVAL METHODS. COMPLETELY UNRELATED KNOWLEDGE IS MARKED IN RED, PARTIALLY RELATED KNOWLEDGE IS MARKED IN PURPLE. RELATED AND IMPORTANT KNOWLEDGE IS IN GREEN.

- [23] K. Singhal, S. Azizi, T. Tu, S. S. Mahdavi, J. Wei, H. W. Chung, N. Scales, A. Tanwani, H. Cole-Lewis, S. Pfohl *et al.*, "Large language models encode clinical knowledge," *arXiv preprint arXiv:2212.13138*, 2022. 2
- [24] C. Raffel, N. Shazeer, A. Roberts, K. Lee, S. Narang, M. Matena, Y. Zhou, W. Li, and P. J. Liu, "Exploring the limits of transfer learning with a unified text-to-text transformer," *The Journal of Machine Learning Research*, vol. 21, no. 1, pp. 5485–5551, 2020. 2
- [25] J. Lee, W. Yoon, S. Kim, D. Kim, S. Kim, C. H. So, and J. Kang, "Bibert: a pre-trained biomedical language representation model for biomedical text mining," *Bioinformatics*, vol. 36, no. 4, pp. 1234–1240, 2020. 2
- [26] Y. Gu, R. Tinn, H. Cheng, M. Lucas, N. Usuyama, X. Liu, T. Naumann, J. Gao, and H. Poon, "Domain-specific language model pretraining for biomedical natural language processing," *ACM Transactions on Computing for Healthcare (HEALTH)*, vol. 3, no. 1, pp. 1–23, 2021. 2
- [27] J. Devlin, M.-W. Chang, K. Lee, and K. Toutanova, "Bert: Pre-training of deep bidirectional transformers for language understanding," *arXiv preprint arXiv:1810.04805*, 2018. 2
- [28] E. Alsentzer, J. R. Murphy, W. Boag, W.-H. Weng, D. Jin, T. Naumann, and M. McDermott, "Publicly available clinical bert embeddings," *arXiv preprint arXiv:1904.03323*, 2019. 2
- [29] T. H. Kung, M. Cheatham, A. Medinilla, ChatGPT, C. Sillos, L. De Leon, C. Elepano, M. Madriaga, R. Aggabao, G. Diaz-Candido *et al.*, "Performance of chatgpt on usml: Potential for ai-assisted medical education using large language models," *medRxiv*, pp. 2022–12, 2022. 2
- [30] A. Radford, J. W. Kim, C. Hallacy, A. Ramesh, G. Goh, S. Agarwal, G. Sastry, A. Askell, P. Mishkin, J. Clark *et al.*, "Learning transferable visual models from natural language supervision," in *International Conference on Machine Learning*. PMLR, 2021, pp. 8748–8763. 2, 3
- [31] X. Chen, X. Wang, S. Changpinyo, A. Piergiovanni, P. Padlewski, D. Salz, S. Goodman, A. Grycner, B. Mustafa, L. Beyer *et al.*, "Pali: A jointly-scaled multilingual language-image model," *arXiv preprint arXiv:2209.06794*, 2022. 2
- [32] W. Wang, H. Bao, L. Dong, J. Bjorck, Z. Peng, Q. Liu, K. Aggarwal, O. K. Mohammed, S. Singhal, S. Som *et al.*, "Image as a foreign language: Beit pretraining for all vision and vision-language tasks," *arXiv preprint arXiv:2208.10442*, 2022. 2
- [33] M. Tsimpoukelli, J. L. Menick, S. Cabi, S. Eslami, O. Vinyals, and F. Hill, "Multimodal few-shot learning with frozen language models," *Advances in Neural Information Processing Systems*, vol. 34, pp. 200–212, 2021. 2
- [34] J.-B. Alayrac, J. Donahue, P. Luc, A. Miech, I. Barr, Y. Hasson, K. Lenc, A. Mensch, K. Millican, M. Reynolds *et al.*, "Flamingo: a visual language model for few-shot learning," *arXiv preprint arXiv:2204.14198*, 2022. 2
- [35] J. Li, D. Li, S. Savarese, and S. Hoi, "Blip-2: Bootstrapping language-image pre-training with frozen image encoders and large language models," *arXiv preprint arXiv:2301.12597*, 2023. 2
- [36] C. Wu, S. Yin, W. Qi, X. Wang, Z. Tang, and N. Duan, "Visual chatgpt: Talking, drawing and editing with visual foundation models," *arXiv preprint arXiv:2303.04671*, 2023. 2

<b>Q3</b> Is pleural effusion serious?
<p><b>K3 (Baseline)</b> Under normal circumstances, a thin layer of pleural fluid (10-20mL) covers the surfaces of the visceral and parietal pleura, with a composition similar to plasma but with lower protein content (<math>&lt;1.5\text{g/dL}</math> [<math>&lt;15\text{ g/L}</math>]). "Etiology": "Abs": "Pleural effusions are usually classified into exudates, transudates, and fluid accumulation based on laboratory characteristics of the fluid (see criteria for diagnosing exudative pleural effusions in the table). Regardless of unilateral or bilateral involvement, leaky effusions usually require little investigation and can be treated, while exudative effusions require identification of the underlying cause. Various factors can cause pleural effusions (see the table for causes of pleural effusions). Leaky pleural effusions are caused by an increase in systemic circulatory hydrostatic pressure and a decrease in plasma colloid osmotic pressure.</p> <p><b>K3 (Ours)</b> Some pleural effusions are asymptomatic and are discovered incidentally during physical examination or on chest x-ray. Many cause dyspnea, pleuritic chest pain, or both. Pleuritic chest pain, a vague discomfort or sharp pain that worsens during inspiration, indicates inflammation of the parietal pleura. Pain is usually felt over the inflamed site, but referred pain is possible. The posterior and peripheral portions of the diaphragmatic pleura are supplied by the lower 6 intercostal nerves, and irritation there may cause pain in the lower chest wall or abdomen that may simulate intra-abdominal disease. Irritation of the central portion of the diaphragmatic pleura, innervated by the phrenic nerves, causes pain referred to the neck and shoulder. Physical examination reveals absent tactile fremitus, dullness to percussion, and decreased breath sounds on the side of the effusion. These findings can also be caused by pleural thickening.</p> <p>...</p> <p>Pericardial rub is best heard over the left border of the sternum in the 3rd and 4th intercostal spaces, is characteristically a to-and-fro sound synchronous with the heartbeat, and is not influenced significantly by respiration. Sensitivity and specificity of the physical examination for detecting effusion are probably low.</p> <p><b>A3 (Ours)</b> The severity of pleural effusion needs to be determined based on the patient's specific situation. Generally, a large amount of effusion can cause symptoms such as dyspnea and chest pain, but some patients may not have obvious symptoms. Physical examination can reveal reduced breath sounds on the effusion side, dullness to percussion, and possibly pleural friction rub. However, the sensitivity and specificity of physical examination for pleural effusion are both low, so clinical symptoms and imaging examinations need to be combined to determine the severity of the effusion and treatment plan. Common causes of pleural effusion include heart failure, pneumonia, and tuberculosis</p>
<b>Q4</b> What should I do after getting lung atelectasis?
<p><b>K4 (Baseline)</b> do not recommend oral or intravenous corticosteroids because they have not shown efficacy in metal fume fever. Patients with pre-existing lung disease (such as asthma or chronic obstructive pulmonary disease) rarely require treatment and hospitalization due to worsening of pre-existing conditions. If severe cases of either syndrome cause respiratory distress, treatment methods used for ARDS (such as mechanical ventilation and positive end-expiratory pressure [PEEP]) may also be used. ", "Atelectasis": "Abs": "Atelectasis is collapse of lung tissue with loss of volume. Patients may have dyspnea or respiratory failure if atelectasis is extensive. They may also develop pneumonia. Atelectasis is usually asymptomatic, but hypoxemia and pleuritic chest pain may be present in certain cases. Diagnosis is by chest x-ray. Treatment includes maintaining coughing and deep breathing and treating the cause."</p> <p><b>K4 (Ours)</b> Maximizing cough and deep breathing If obstruction by tumor or foreign body is suspected, bronchoscopy Evidence for the efficacy of most treatments for atelectasis is weak or absent. Nonetheless, commonly recommended measures include chest physiotherapy to help maintain ventilation and clearance of secretions, and encouragement of lung expansion techniques such as directed cough, deep breathing exercises, and use of an incentive spirometer. In ambulatory patients, exercise (eg, walking) is a desirable way to promote deep breathing. For patients who are not intubated and do not have excessive secretions, continuous positive airway pressure may help. For patients who are intubated and mechanically ventilated, positive end-expiratory pressure and/or higher tidal volume ventilation may help.</p> <p>...</p> <p>If other measures are ineffective or if a cause of obstruction other than mucous plugging is suspected, bronchoscopy should be done.</p> <p><b>A4 (Ours)</b> The treatment methods for pulmonary atelectasis include maintaining cough and deep breathing, chest physical therapy, exercise, continuous positive airway pressure, etc. However, the evidence for the effectiveness of these treatments is not sufficient, so the treatment plan needs to be developed according to the specific situation of the patient. If there is suspicion of tumor or foreign body obstruction, bronchoscopy examination is needed. Opioid drugs can be used to relieve severe pleural pain, but cough suppressant drugs should be avoided. For the causes of pulmonary atelectasis such as mucus plugs, foreign bodies, tumors, masses, pleural effusions, etc., targeted treatments should be used.</p>

TABLE V

COMPARISON BETWEEN KNOWLEDGE RETRIEVAL METHODS. COMPLETELY UNRELATED KNOWLEDGE IS MARKED IN RED, PARTIALLY RELATED KNOWLEDGE IS MARKED IN PURPLE. RELATED AND IMPORTANT KNOWLEDGE IS IN GREEN.

- [37] S. Liu, Z. Zeng, T. Ren, F. Li, H. Zhang, J. Yang, C. Li, J. Yang, H. Su, J. Zhu, and L. Zhang, "Grounding dino: Marrying dino with grounded pre-training for open-set object detection," 2023. **3**
- [38] A. Kirillov, E. Mintun, N. Ravi, H. Mao, C. Rolland, L. Gustafson, T. Xiao, S. Whitehead, A. C. Berg, W.-Y. Lo, P. Dollár, and R. Girshick, "Segment anything," *arXiv:2304.02643*, 2023. **3**
- [39] J. L. Bentley, "Multidimensional binary search trees used for associative searching," *Communications of the ACM*, vol. 18, no. 9, pp. 509–517, 1975. **4**
- [40] A. E. Johnson, T. J. Pollard, S. J. Berkowitz, N. R. Greenbaum, M. P. Lungren, C.-y. Deng, R. G. Mark, and S. Horng, "Mimic-cxr, a de-identified publicly available database of chest radiographs with free-text reports," *Scientific data*, vol. 6, no. 1, p. 317, 2019. **5**
- [41] W. Ye, J. Yao, H. Xue, and Y. Li, "Weakly supervised lesion localization with probabilistic-cam pooling," 2020. **5**
- [42] J. Irvin, P. Rajpurkar, M. Ko, Y. Yu, S. Ciurea-Ilcus, C. Chute, H. Marklund, B. Haghighi, R. Ball, K. Shpanskaya *et al.*, "Chexpert: A large chest radiograph dataset with uncertainty labels and expert comparison," in *Proceedings of the AAAI conference on artificial intelligence*, vol. 33, no. 01, 2019, pp. 590–597. **5**
- [43] L. Mei, Y. Fang, Z. Cui, K. Deng, N. Wang, X. He, Y. Zhan, X. Zhou, M. Tonetti, and D. Shen, "Hc-net: Hybrid classification network for automatic periodontal disease diagnosis," in *Medical Image Computing and Computer Assisted Intervention-MICCAI 2023: 26th International Conference, Vancouver*. Springer, 2023. **5**
- [44] K. Papineni, S. Roukos, T. Ward, and W.-J. Zhu, "Bleu: a method for automatic evaluation of machine translation," in *Proceedings of the 40th annual meeting of the Association for Computational Linguistics*, 2002, pp. 311–318. **6**
- [45] S. Banerjee and A. Lavie, "Meteor: An automatic metric for mt evaluation with improved correlation with human judgments," in *Proceedings of the acl workshop on intrinsic and extrinsic evaluation measures for machine translation and/or summarization*, 2005, pp. 65–72. **6**
- [46] C.-Y. Lin, "Rouge: A package for automatic evaluation of summaries," in *Text summarization branches out*, 2004, pp. 74–81. **6**
- [47] A. Smit, S. Jain, P. Rajpurkar, A. Pareek, A. Y. Ng, and M. P. Lungren, "Chexpert: combining automatic labelers and expert annotations for accurate radiology report labeling using bert," *arXiv preprint arXiv:2004.09167*, 2020. **6**
- [48] langchain ChatGLM Contributors, "Chatglm application with local knowledge implementation," <https://github.com/imClumsyPanda/langchain-ChatGLM>, 2023. **6**
- [49] M. Denkowski and A. Lavie, "Meteor 1.3: Automatic metric for reliable optimization and evaluation of machine translation systems," in *Proceedings of the Sixth Workshop on Statistical Machine Translation*. Edinburgh, Scotland: Association for Computational Linguistics, Jul. 2011, pp. 85–91. [Online]. Available: <https://aclanthology.org/W11-2107> **7**
- [50] K. Chaitanya, E. Erdil, N. Karani, and E. Konukoglu, "Contrastive learning of global and local features for medical image segmentation with limited annotations," *arXiv preprint arXiv:2006.10511*, 2020. **8**